

# Electronic Structure and Metal–Metal Interactions in Trinuclear Face-Shared $[M_3X_{12}]^{3-}$ ( $M = Mo, W; X = F, Cl, Br, I$ ) Systems

Germán Cavigliasso and Robert Stranger\*

Department of Chemistry, Faculty of Science, Australian National University, Canberra ACT 0200, Australia

Received October 19, 2007

The molecular and electronic structures of trinuclear face-shared  $[M_3X_{12}]^{3-}$  species of Mo ( $X = F, Cl, Br, I$ ) and W ( $X = Cl$ ), containing linear chains of metal atoms, have been investigated using density functional theory. The possibility of variations in structure and bonding has been explored by considering both symmetric ( $D_{3d}$ ) and unsymmetric ( $C_{3v}$ ) forms, the latter having one long and one short metal–metal distance. Analysis of the bonding in the structurally characterized  $[Mo_3I_{12}]^{3-}$  trimer reveals that the metal–metal interaction qualitatively corresponds to a two-electron three-center  $\sigma$  bond between the Mo atoms and, consequently, a formal Mo–Mo bond order of 0.5. However, the calculated spin densities suggest that the electrons in the metal–metal  $\sigma$  bond are not fully decoupled and therefore participate in the antiferromagnetic interactions of the metal cluster. Although the same observation applies to  $[Mo_3X_{12}]^{3-}$  ( $X = Br, Cl, F$ ) and  $[W_3Cl_{12}]^{3-}$ , both the spin densities and shorter distances between the metal atoms indicate that the metal–metal interaction is stronger in these systems. The broken-symmetry approach combined with spin projection has been used to determine the energy of the low-lying spin multiplets arising from the magnetic coupling between the metal centers. Either the symmetric and unsymmetric  $S = 3/2$  state is predicted to be the ground state for all five systems. For  $[Mo_3X_{12}]^{3-}$  ( $X = Cl, Br, I$ ), the symmetric form is more stable but the unsymmetric structure, where two metal centers are involved in a metal–metal triple bond while the third center is decoupled, lies close in energy and is thermally accessible. Consequently, at room temperature, interconversion between the two energetically equivalent configurations of the unsymmetric form should result in an averaged structure that is symmetric. This prediction is consistent with the reported structure of  $[Mo_3I_{12}]^{3-}$ , which, although symmetric, indicates significant movement of the central Mo atom toward the terminal Mo atoms on either side. In contrast, unsymmetric structures with a triple bond between two metal centers are predicted for  $[Mo_3F_2]^{3-}$  and  $[W_3C_{12}]^{3-}$ , as the symmetric structure lies too high in energy to be thermally accessible.

## 1. Introduction

The electronic structure of trinuclear metal complexes containing linear chains of metal atoms has been the subject of significant theoretical and computational interest, largely due to the observed structural variation associated with the possibility of these systems displaying “bond stretch isomerism”,<sup>1,2</sup> the phenomenon whereby a molecule can exist in two distinct structural forms but having the same spin state. Among the most representative examples are species of the type  $[M_3(dpa)L_2]$  or  $[M_3(dpa)LL']$ , where M is Co or Cr, dpa is the dipyrrolic

amide anion, and L and L' are halogen atoms or molecular anions.<sup>3–7</sup> A distinctive feature of the complexes formed by both Co and Cr is the presence of a metal-based three-electron three-center bond, in which the unpaired electron occupies a nonbonding orbital.<sup>1</sup>

\* To whom correspondence should be addressed. E-mail: rob.stranger@anu.edu.au.

(1) Rohmer, M.-M.; Bénard, M. *Chem. Soc. Rev.* **2001**, 30, 340.  
(2) Pantazis, D. A.; McGrady, J. E. *J. Am. Chem. Soc.* **2006**, 128, 4128.

(3) Clérac, R.; Cotton, F. A.; Daniels, L. M.; Dunbar, K. R.; Murillo, C. A.; Pascual, I. *Inorg. Chem.* **2000**, 39, 748.  
(4) Clérac, R.; Cotton, F. A.; Dunbar, K. R.; Lu, T. B.; Murillo, C. A.; Wang, X. *J. Am. Chem. Soc.* **2000**, 122, 2272.  
(5) Clérac, R.; Cotton, F. A.; Daniels, L. M.; Dunbar, K. R.; Kirschbaum, K.; Murillo, C. A.; Pinkerton, A. A.; Schultz, A. J.; Wang, X. *J. Am. Chem. Soc.* **2000**, 122, 6226.  
(6) Clérac, R.; Cotton, F. A.; Daniels, L. M.; Dunbar, K. R.; Murillo, C. A.; Wang, X. *Inorg. Chem.* **2001**, 40, 1256.  
(7) Berry, J. F.; Cotton, F. A.; Lu, T.; Murillo, C. A.; Roberts, B. K.; Wang, X. *J. Am. Chem. Soc.* **2004**, 126, 7082.

Trinuclear  $[M_3X_{12}]^{3-}$  ( $X = \text{Cl, Br, I}$ ) systems containing linear chains of Mo atoms have also been reported.<sup>8,9</sup> These species can display variation in their structural properties and in the nature of metal–metal bonding, but no computational studies using high-level theory have been performed to investigate these aspects of their chemistry. The experimental characterization of an analogous ruthenium halide ( $[\text{Ru}_3\text{Cl}_{12}]^{4-}$ ) complex has been reported,<sup>10</sup> and a computational investigation of its electronic structure has been carried out,<sup>11</sup> but only using much more approximate methods.

The theoretical and computational treatment of polynuclear metal complexes involving halide bridging ligands is particularly challenging due to the considerable variation in structural, electronic, and magnetic properties resulting from the competing effects of the metal–metal and metal-bridge interactions. Nevertheless, in a recent series of publications<sup>12–26</sup> covering a large and diverse set of dinuclear face-shared  $[M_2X_9]^{2-}$  and edge-shared  $[M_2X_{10}]^{2-}$  systems, we have shown that density functional theory, in combination with the broken-symmetry approach of Noodleman and co-workers,<sup>27,28</sup> can accurately describe the entire range of metal–metal interactions, from weak antiferromagnetic coupling through to multiple metal–metal bonding, as well as encompassing both high-spin and low-spin metal configurations.

In this article, we apply the same methodology to the study of the electronic structure and metal–metal interactions in trinuclear face-shared  $[M_3X_{12}]^{3-}$  systems, with a focus on the crystallographically characterized  $[\text{Mo}_3\text{I}_{12}]^{3-}$  species. For comparative purposes, we also consider  $[\text{Mo}_3\text{F}_{12}]^{3-}$ ,  $[\text{Mo}_3\text{Cl}_{12}]^{3-}$ ,  $[\text{Mo}_3\text{Br}_{12}]^{3-}$ , and  $[\text{W}_3\text{Cl}_{12}]^{3-}$ . Potential energy curves for various spin states corresponding to the symmetric ( $D_{3d}$ ) forms are described and analyzed, and the possibility of structural variation is also explored by investigating the unsymmetric ( $C_{3v}$ ) forms. In addition, the broken-symmetry approach combined with spin-projection techniques is used to predict the energy of the low-lying spin states and rationalize the magnetic properties of these complexes.

## 2. Calculation Details

All density functional calculations reported in this article were carried out with the Amsterdam Density Functional (ADF) package.<sup>29–31</sup> Functionals based on the Volko–Wilk–Nusair (VWN) form<sup>32</sup> of the local density approximation (LDA),<sup>33</sup> and the generalized-gradient-approximation (GGA) forms involving the exchange expression proposed by Becke (labeled B)<sup>34</sup> and the correlation expression proposed by Perdew (labeled P),<sup>35</sup> or the exchange and correlation expressions due to Perdew, Burke, and Ernzerhof<sup>36</sup> (labeled PBE), were utilized. Basis sets of triple- $\zeta$  quality and one (TZP) or two (TZ2P) polarization functions, incorporating frozen cores (W.4f, Mo.3d, I.4p, Br.3p, Cl.2p, F.1s), were employed.<sup>29–31</sup> Relativistic effects were included by means of the zero-order regular approximation (ZORA),<sup>37–39</sup> and the conductor-like screening model (COSMO) was used for the treatment of solvation effects.<sup>40</sup> Default convergence parameters were used for self-consistent-field (SCF) procedures (integration accuracy of 4.0) and geometry optimizations (gradient tolerance of 0.01). Frequency calculations were carried out using both numerical differentiation of gradients<sup>41,42</sup> and analytical second derivatives,<sup>43–45</sup> with both procedures requiring an integration accuracy of 6.0 and the geometry optimization step preceding the analytical approach, a gradient tolerance parameter of 0.0001. Plots of the molecular orbitals were generated with the MOLEKEL program<sup>46,47</sup> using data in MOLDEN-format<sup>48,49</sup> derived from the ADF TAPE21 files.

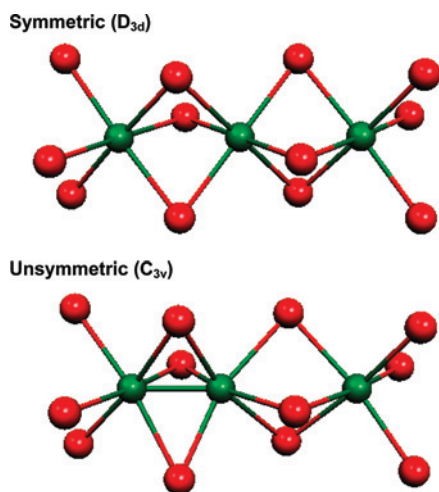
## 3. Results and Discussion

The molecular structure of the symmetric form of the face-shared  $[M_3X_{12}]^{3-}$  systems (shown in Scheme 1) is character-

- (8) Fettinger, J. C.; Gordon, J. C.; Mattamana, S. P.; O'Connor, C. J.; Poli, R.; Salem, G. *Inorg. Chem.* **1996**, *35*, 7404.
- (9) Delphin, W. H.; Wentworth, R. A. D.; Matson, M. S. *Inorg. Chem.* **1974**, *13*, 2552.
- (10) Bino, A.; Cotton, F. A. *J. Am. Chem. Soc.* **1980**, *102*, 608.
- (11) Bursten, B. E.; Cotton, F. A.; Fang, A. *Inorg. Chem.* **1983**, *22*, 2127.
- (12) Lovell, T.; McGrady, J. E.; Stranger, R.; Macgregor, S. A. *Inorg. Chem.* **1996**, *35*, 3079.
- (13) McGrady, J. E.; Stranger, R.; Lovell, T. *J. Phys. Chem. A* **1997**, *101*, 6265.
- (14) Stranger, R.; McGrady, J. E.; Lovell, T. *Inorg. Chem.* **1998**, *37*, 6795.
- (15) Lovell, T.; Stranger, R.; McGrady, J. E. *Inorg. Chem.* **2001**, *40*, 39.
- (16) Stranger, R.; Turner, A.; Delfs, C. D. *Inorg. Chem.* **2001**, *40*, 4093.
- (17) Petric, S.; Stranger, R. *Polyhedron* **2002**, *21*, 1163.
- (18) Stranger, R.; Lovell, T.; McGrady, J. E. *Polyhedron* **2002**, *21*, 1969.
- (19) Cavigliasso, G.; Stranger, R. *Inorg. Chem.* **2003**, *42*, 5252.
- (20) Cavigliasso, G.; Stranger, R. *Inorg. Chem.* **2004**, *43*, 2368.
- (21) Cavigliasso, G.; Comba, P.; Stranger, R. *Inorg. Chem.* **2004**, *43*, 6734.
- (22) Cavigliasso, G.; Stranger, R. *Inorg. Chem.* **2005**, *44*, 5081.
- (23) McGrady, J. E.; Stranger, R.; Lovell, T. *Inorg. Chem.* **1998**, *37*, 3802.
- (24) Stranger, R.; Lovell, T.; McGrady, J. E. *Inorg. Chem.* **1999**, *38*, 5510.
- (25) Cavigliasso, G.; Lovell, T.; Stranger, R. *J. Chem. Soc., Dalton Trans.* **2006**, 2017.
- (26) Cavigliasso, G.; Yu, C.-Y.; Stranger, R. *Polyhedron* **2007**, *26*, 2942.
- (27) Noodleman, L.; Norman, J. G. *J. Chem. Phys.* **1979**, *70*, 4903.
- (28) Noodleman, L. *J. Chem. Phys.* **1981**, *74*, 5737.

- (29) ADF, SCM, Theoretical Chemistry. Vrije Universiteit: Amsterdam, The Netherlands <http://www.scm.com>.
- (30) Fonseca Guerra, C.; Snijders, J. G.; te Velde, G.; Baerends, E. J. *Theor. Chem. Acc.* **1998**, *99*, 391.
- (31) te Velde, G.; Bickelhaupt, F. M.; van Gisbergen, S. J. A.; Fonseca Guerra, C.; Baerends, E. J.; Snijders, J. G.; Ziegler, T. *J. Comput. Chem.* **2001**, *22*, 931.
- (32) Vosko, S. H.; Wilk, L.; Nusair, M. *Can. J. Phys.* **1980**, *58*, 1200.
- (33) Kohn, W.; Sham, L. J. *Phys. Rev.* **1965**, *140*, A1133.
- (34) Becke, A. D. *Phys. Rev. A* **1988**, *38*, 3098.
- (35) Perdew, J. P. *Phys. Rev. B* **1986**, *33*, 8822.
- (36) Perdew, J. P.; Burke, K.; Ernzerhof, M. *Phys. Rev. Letters*, **1996**, *77*, 3865.
- (37) van Lenthe, E.; Baerends, E. J.; Snijders, J. G. *J. Chem. Phys.* **1993**, *99*, 4597.
- (38) van Lenthe, E.; Baerends, E. J.; Snijders, J. G. *J. Chem. Phys.* **1994**, *101*, 9783.
- (39) van Lenthe, E.; Ehlers, A. E.; Baerends, E. J. *J. Chem. Phys.* **1999**, *110*, 8943.
- (40) Pye, C. C.; Ziegler, T. *Theor. Chem. Acc.* **1999**, *101*, 396.
- (41) Fan, L.; Ziegler, T. *J. Chem. Phys.* **1992**, *96*, 9005.
- (42) Fan, L.; Ziegler, T. *J. Phys. Chem.* **1992**, *96*, 6937.
- (43) Bérces, A.; Dickson, R. M.; Fan, L.; Jacobsen, H.; Swerhone, D.; Ziegler, T. *Comput. Phys. Commun.* **1997**, *100*, 247.
- (44) Jacobsen, H.; Bérces, A.; Swerhone, D.; Ziegler, T. *Comput. Phys. Commun.* **1997**, *100*, 263.
- (45) Wolff, S. K. *Int. J. Quantum Chem.* **2005**, *104*, 645.
- (46) MOLEKEL: An Interactive Molecular Graphics Tool. <http://www.cscs.ch/molekel/>.
- (47) Portmann, S.; Lüthi, H. P. *Chimia* **2000**, *54*, 766.
- (48) MOLDEN: A Pre and Post Processing Program for Molecular and Electronic Structures. <http://www.cmbi.ru.nl/molden/molden.html>.
- (49) Schaftenaar, G.; Noordik, J. H. *J. Comput. Aided Mol. Design* **2000**, *14*, 123.

Scheme 1



ized by  $D_{3d}$  symmetry, with the metal sites lying in a distorted octahedral environment having  $C_{3v}$  local symmetry. In the  $C_{3v}$  point group, the occupied metal-based  $t_{2g}$  orbitals relevant to the metal–metal interactions transform as the  $a_1$  and  $e$  representations, respectively. These orbitals can participate in  $\sigma$  and  $\delta_\pi$  overlap with adjacent metal centers, where the  $\delta_\pi$  label is used to indicate the mixed ( $^2/3\delta + ^1/3\pi$ ) character due to the local trigonal symmetry, in analogous fashion to their dinuclear face-shared  $[M_2X_9]^{2-}$  counterparts.<sup>13,16</sup> In the delocalized bonding model, the metal–metal interactions involving the  $t_{2g}$  orbitals give rise to  $a_{1g}$ ,  $e_g$ ,  $e_u$ ,  $a_{2u}$ ,  $e_g$ , and  $a_{1g}$  molecular orbitals. The relative energies and spatial plots of these orbitals are shown in Figure 1 for the optimized  $D_{3d}$  geometry of  $[Mo_3I_{12}]^{3-}$ . The low-lying and high-lying  $a_{1g}$  orbitals exhibit, respectively,  $\sigma$ -bonding and  $\sigma$ -antibonding character between adjacent metal atoms, whereas the major contributions to the composition of the  $e_g$ ,  $e_u$ , and  $a_{2u}$  orbitals originate from either the central or terminal sites, and therefore, these levels can be considered to be largely nonbonding between the metal atoms.

Fettinger and co-workers<sup>8</sup> have suggested that the experimentally characterized structure of  $[Mo_3I_{12}]^{3-}$  contains a two-electron three-center metal–metal bond across the linear chain of Mo atoms. This bonding situation results from two electrons occupying the low-lying  $a_{1g}$   $\sigma$ -bonding orbital while the seven remaining electrons reside in the largely nonbonding  $e_g$ ,  $e_u$ , and  $a_{2u}$  levels, and leads to a formal metal–metal bond order of 0.5. The plots of the molecular orbitals for  $[Mo_3I_{12}]^{3-}$  shown in Figure 1 are qualitatively in agreement with this analysis, but the actual metal–metal interaction may be weaker than the formal description suggests due to the relatively long metal–metal distance of approximately 3.34 Å at the energy minimum.

Due to the individual  $d^3$  metal configurations, the occupation of the  $t_{2g}$  orbitals in  $C_{3v}$  local symmetry is  $[(a_1)^1(e)^2]$ . The resulting  $[d^3d^3d^3]$  coupling mode for the trimer can therefore be described as  $[(a_1)^1(e)^2 \times (a_1)^1(e)^2 \times (a_1)^1(e)^2]$ , which gives rise to a number of low-lying spin states ranging from  $S = 1/2$  to  $S = 9/2$ . The majority of these spin states cannot be represented by single-electron configurations, and therefore, their energies are not amenable to calculation by

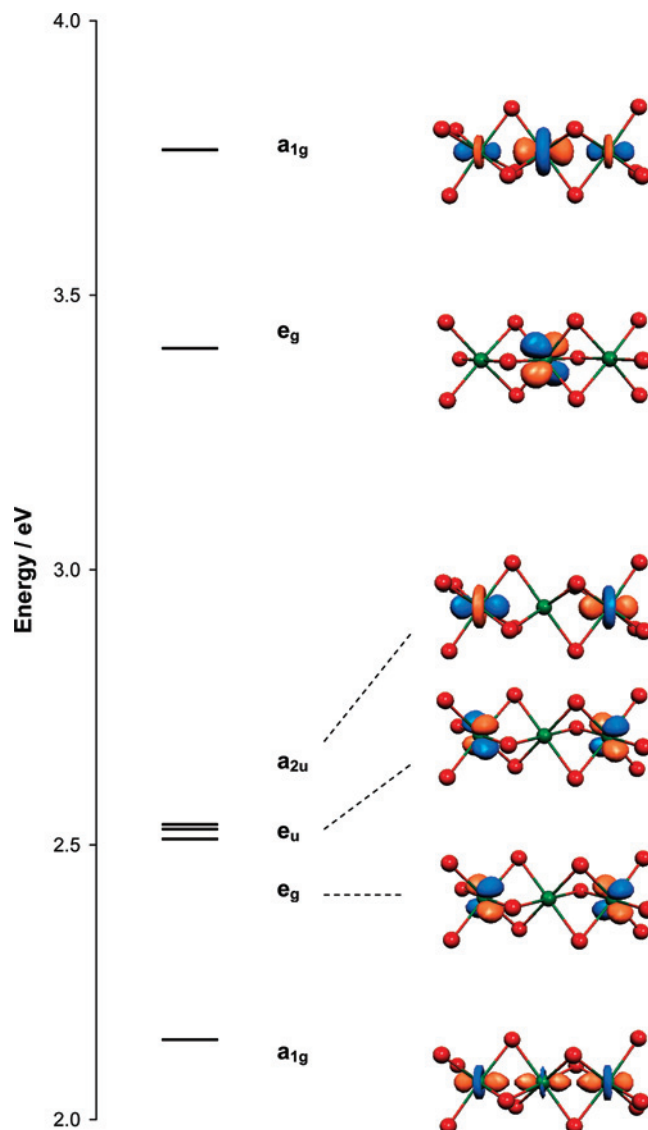


**Figure 1.** Molecular orbital plots for the symmetric forms (broken-symmetry configuration) of the  $[Mo_3I_{12}]^{3-}$  species.

density functional methods. However, the  $S = 9/2$  state, where all metal-based electrons are aligned parallel, and the  $S = 7/2$  state, where two electrons are paired in a metal–metal  $\sigma$  bond while the remaining electrons are aligned parallel, can be described by single configurations. In addition to these two spin states, there are antiferromagnetic (broken-symmetry) states that can also be represented by single configurations. These states are best considered in the context of a localized model and can be constructed by aligning the unpaired spins on adjacent metal centers in either a parallel or antiparallel manner such that the total  $M_S$  value is  $3/2$ . Of relevance to this discussion is the broken-symmetry (BS) state that results when the electrons on the central metal atom are aligned antiparallel to those on the terminal metal centers. Although this broken-symmetry state has  $M_S = 3/2$ , it is not a pure spin state but rather a weighted average of spin states with  $S \geq 3/2$ . A schematic representation of the localized  $C_{3v}$  and delocalized  $D_{3d}$  molecular-orbital descriptions of the broken-symmetry,  $S = 7/2$ , and  $S = 9/2$  states is shown in Figure 2. In the delocalized limit, the BS,  $S = 7/2$ , and  $S = 9/2$

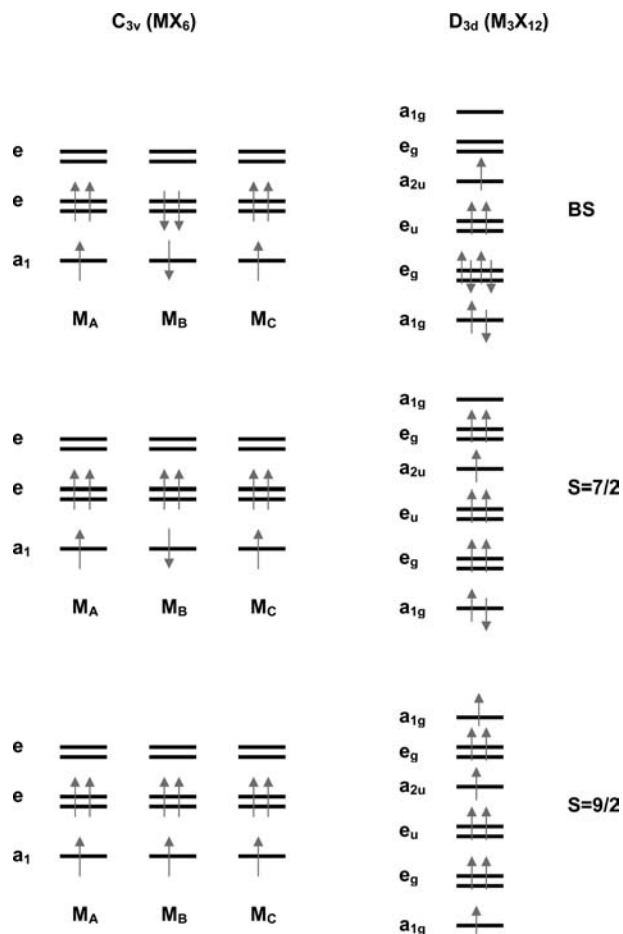


**Figure 2.** Correlation between the  $C_{3v}$  and  $D_{3d}$  molecular orbital descriptions of the symmetric forms of  $[M_3X_{12}]^{3-}$  species.

$= 9/2$  states can be correlated with the following  $D_{3d}$  molecular-orbital configurations,

$$\begin{aligned} \text{BS} & [(a_{1g})^2(e_g)^4(e_u)^2(a_{2u})^1(e_g)^0(a_{1g})^0] \\ S=7/2 & [(a_{1g})^2(e_g)^2(e_u)^2(a_{2u})^1(e_g)^2(a_{1g})^0] \\ S=9/2 & [(a_{1g})^1(e_g)^2(e_u)^2(a_{2u})^1(e_g)^2(a_{1g})^1] \end{aligned}$$

with the molecular orbital plots in Figure 1 corresponding to the broken-symmetry configuration.

**3.1. Computational Methodology Tests.** In our investigations of dinuclear metal complexes,<sup>12–26</sup> we have been able to successfully describe the entire range of metal–metal interactions displayed by these systems using the local density approximation. The effectiveness of this method is exemplified by the fact that our calculations have satisfactorily reproduced the observed properties of a large number of face-shared  $[M_2X_9]^{z-}$  species, with electronic configurations ranging from  $d^1d^1$  through to  $d^5d^5$ , as well as mixed-valence  $d^1d^2$ ,  $d^2d^3$ ,  $d^3d^4$ , and  $d^4d^5$  configurations, and also of a variety of other dimer systems including edge-shared  $[M_2X_{10}]^{z-}$  and phosphine-bridged  $[M_2X_6(P-P)_4]^{z-}$  species.

The use of the local density approximation (LDA) is supported by results from a recent comparative study<sup>50</sup> on the performance of various density functionals in the

**Table 1.** Comparison of Optimized Metal–Metal Distances (Å) for the BS,  $S = 0$ ,  $S = 2$ , and  $S = 3$  States of  $[Mo_2Cl_9]^{3-}$ ,  $[Mo_2Br_9]^{3-}$ , and  $[W_2Cl_9]^{3-}$

molecule	method <sup>a</sup>	BS	$S = 0$	$S = 2$	$S = 3$
$[Mo_2Cl_9]^{3-}$ <sup>b</sup>	LDA/TZP	2.38	2.37	2.83	3.41
	BP/ZC/TZP	2.76	2.38	2.82	3.40
	BP/ZC/TZ2P	2.69	2.33	2.79	3.38
	PBE/ZC/TZP	2.74	2.37	2.81	3.39
$[Mo_2Br_9]^{3-}$ <sup>c</sup>	LDA/TZP	2.43	2.40	2.91	3.55
	PBE/ZC/TZ2P	2.85	2.35	2.85	3.49
$[W_2Cl_9]^{3-}$ <sup>d</sup>	LDA/TZP	2.44	2.43	2.86	3.43
	PBE/ZC/TZ2P	2.39	2.38	2.78	3.38

<sup>a</sup> The ZC label indicates inclusion of ZORA and COSMO corrections. <sup>b</sup> Experimental Mo–Mo distance in  $[A_3Mo_2Cl_9]$  ( $A = K, Rb, Cs, NH_4$ ) is 2.52–2.66 Å.<sup>54</sup> <sup>c</sup> Experimental Mo–Mo distance in  $[A_3Mo_2Br_9]$  ( $A = K, Rb, Cs$ ) is 2.57–2.82 Å.<sup>54</sup> <sup>d</sup> Experimental W–W distance in  $[A_3W_2Cl_9]$  ( $A = \text{organic cation}$ ) is 2.43 Å.<sup>56</sup>

**Table 2.** Comparison of Calculated Total Bonding Energy Data (eV) for the BS,  $S = 0$ ,  $S = 2$ , and  $S = 3$  States of  $[Mo_2Cl_9]^{3-}$ ,  $[Mo_2Br_9]^{3-}$ , and  $[W_2Cl_9]^{3-}$

molecule	method <sup>a</sup>	BS	$S = 0$	$S = 2$	$S = 3$
$[Mo_2Cl_9]^{3-}$	LDA/TZP	−51.41	−51.41	−51.17	−50.78
	BP/ZC/TZP	−61.20	−60.94	−60.98	−60.79
	BP/ZC/TZ2P	−62.00	−61.89	−61.78	−61.52
	PBE/ZC/TZP	−61.69	−61.47	−61.47	−61.23
$[Mo_2Br_9]^{3-}$	LDA/TZP	−47.19	−47.18	−47.00	−46.74
	PBE/ZC/TZ2P	−57.10	−56.97	−56.90	−56.69
$[W_2Cl_9]^{3-}$	LDA/TZP	−53.21	−53.21	−52.71	−52.06
	PBE/ZC/TZ2P	−61.91	−61.91	−61.24	−60.42

<sup>a</sup> The ZC label indicates inclusion of ZORA and COSMO corrections.

calculation of metal–metal distances for a diverse set of molecular complexes. This study has shown that a better description of the metal–metal interactions is achieved by LDA rather than gradient-corrected functionals for systems carrying a relatively high molecular charge.

In the present work, in addition to methodology based on the local density approximation, we have employed approaches that involve the combination of gradient-corrected forms with a treatment for relativistic effects (using ZORA procedures) as these have been shown<sup>51</sup> to provide a satisfactory description of negatively charged metal–metal bonded complexes. In addition, solvent effects (using the COSMO solvation model) have also been incorporated into these calculations, as it has been recently shown that their inclusion leads to better agreement with the available structural data for (highly charged) anionic species.<sup>52,53</sup>

As an initial test on the performance of the local-density and gradient-corrected (ZORA/COSMO) approaches, the structures and energetics of the well-known  $[Mo_2Cl_9]^{3-}$ ,  $[Mo_2Br_9]^{3-}$ , and  $[W_2Cl_9]^{3-}$  dimer systems were calculated, and the results are summarized in Tables 1 and 2. Detailed descriptions of the relevant broken-symmetry (BS) and associated ( $S = 0$ ,  $S = 2$ ,  $S = 3$ ) states for these species have been presented in previous publications.<sup>13,16,19</sup>

(51) Cavigliasso, G.; Kaltsoyannis, N. *J. Chem. Soc., Dalton Trans.* **2006**, 5476.

(52) Hocking, R. K.; Deeth, R. J.; Hambley, T. W. *Inorg. Chem.* **2007**, *46*, 8238.

(53) López, X.; Fernández, J. A.; Romo, S.; Paul, J. F.; Kazansky, L.; Poblet, J. M. *J. Comput. Chem.* **2004**, *25*, 1542.

(50) Petrie, S.; Stranger, R. *Inorg. Chem.* **2004**, *43*, 2597.

For  $[\text{Mo}_2\text{Cl}_9]^{3-}$ , all methods tested show similar trends in the metal–metal distances predicted for the associated states, but noticeable differences are found for the broken-symmetry state. Although the gradient-corrected results in Table 1 for the broken-symmetry state are in good agreement with the experimental metal–metal distances for  $[\text{A}_3\text{Mo}_2\text{Cl}_9]$  ( $\text{A} = \text{K}, \text{Rb}, \text{Cs}, \text{NH}_4$ ) salts, the corresponding value obtained using the local density approximation is less satisfactory. However, it should be noted that the potential energy curve for  $[\text{Mo}_2\text{Cl}_9]^{3-}$  is considerably flat in the vicinity of the minimum, and the total bonding energy values obtained from LDA calculations at Mo–Mo distances between 2.5 and 2.9 Å are largely similar to that corresponding to the minimum at approximately 2.4 Å.

The correct energetic ordering for the associated states, represented by

$$E(S=0) < E(S=2) < E(S=3)$$

is reproduced by the [LDA/TZP] calculations (Table 2), but the results obtained using gradient-corrected functionals are only satisfactory if the larger TZ2P basis sets are employed. The additional calculations performed on the  $[\text{Mo}_2\text{Br}_9]^{3-}$  and  $[\text{W}_2\text{Cl}_9]^{3-}$  systems confirm that the same structural and energetic trends for the associated states are produced by the simple [LDA/TZP] approach as the more complex (and computationally demanding) [PBE/ZC/TZ2P] procedure. As noted for  $[\text{Mo}_2\text{Cl}_9]^{3-}$ , the discrepancies in the broken-symmetry results for  $[\text{Mo}_2\text{Br}_9]^{3-}$  are due to the flatness of the potential energy curve for Mo–Mo separations between 2.3 and 2.9 Å.

An additional test of method performance is provided by a calculation of the exchange coupling ( $J$ ) constant, which can be obtained from the energy difference between the  $S_{\text{max}}$  and broken-symmetry (BS) states using the following expression<sup>13</sup>

$$E(S_{\text{max}}) - E(\text{BS}) = -S_{\text{max}}^2 J \quad (1)$$

where the  $S = S_{\text{max}}$  state for the dimer systems corresponds to the  $S = 2$  state, characterized by the presence of a metal–metal  $\sigma$  bond but only weakly coupled  $\delta_\pi$  electrons. The experimentally determined  $J$  values<sup>54</sup> for  $[\text{A}_3\text{Mo}_2\text{Cl}_9]$  ( $\text{A} = \text{K}, \text{Rb}, \text{Cs}, \text{NH}_4$ ) salts lie in the range of  $-414$  to  $-560$   $\text{cm}^{-1}$ , with the average corresponding to  $-484$   $\text{cm}^{-1}$ , and for  $[\text{Cs}_3\text{Mo}_2\text{Br}_9]$ , the observed  $J$  value is  $-380$   $\text{cm}^{-1}$ . The  $J$  values predicted by the [LDA/TZP] calculations are  $-484$  and  $-374$   $\text{cm}^{-1}$  for  $[\text{Mo}_2\text{Cl}_9]^{3-}$  and  $[\text{Mo}_2\text{Br}_9]^{3-}$ , respectively, in excellent agreement with the experimental observations. The corresponding results from the [PBE/ZC/TZ2P] calculations are  $-439$  and  $-421$   $\text{cm}^{-1}$ , respectively, and show reasonable agreement with experiment but are not as good as those obtained from the [LDA/TZP] calculations.

A final comparative assessment of computational predictions is given in Table 3, where optimized metal–metal distances and total bonding energy values, obtained with [LDA/TZP] and [PBE/ZC/TZ2P] procedures, are shown for the BS,  $S = 7/2$ , and  $S = 9/2$  states of the symmetric form of  $[\text{Mo}_3\text{I}_{12}]^{3-}$ , which has been crystallographically characterized, and exhibits a Mo–Mo bond length of 3.258 Å.<sup>8</sup> As observed

**Table 3.** Optimized Metal–Metal Distance (M–M in angstroms) and Total Bonding Energy ( $E_{\text{B}}$  in electronvolts) for the BS,  $S = 7/2$ , and  $S = 9/2$  States of  $[\text{Mo}_3\text{I}_{12}]^{3-}$  in (Full)  $D_{3d}$  Symmetry

parameter	state	LDA/TZP	PBE/ZC/TZ2P <sup>a</sup>
M–M	BS	3.337	3.306
	$S = 7/2$	3.214	3.182
	$S = 9/2$	3.643	3.623
$E_{\text{B}}$	BS	−61.18	−67.74
	$S = 7/2$	−61.08	−67.57
	$S = 9/2$	−60.72	−67.31

<sup>a</sup> The ZC label indicates inclusion of ZORA and COSMO corrections.

in the case of the dimer systems, the same structural and energetic trends are produced whether the local density approximation or the gradient-corrected functional is used.

The overall results described in this section show that the LDA-based methodology is a satisfactory approach to the calculation of the structures, energetics, and magnetic properties of dimer and trimer species that exhibit metal–metal bonding interactions. Since the current investigations involve obtaining potential energy curves for several states and systems, from a computational performance viewpoint, the LDA-based methodology is also a more convenient choice than the significantly more demanding gradient-corrected approaches (which, in addition, require inclusion of relativistic and solvent treatments and larger basis sets to yield satisfactory results). Consequently, the work reported in sections 3.2–3.4 is based on the [LDA/TZP] calculations, but, for comparative purposes, results from [PBE/ZC/TZ2P] calculations are also presented in section 3.5.

**3.2. Symmetric Structures.** Potential energy curves for the BS,  $S = 7/2$ , and  $S = 9/2$  states as a function of metal–metal separation are shown in Figure 3 for the symmetric ( $D_{3d}$ ) structures of the Mo ( $X = \text{I}, \text{Cl}, \text{F}$ ) and W ( $X = \text{Cl}$ ) systems, while the optimized metal–metal distances corresponding to the minima in these curves are given in Table 4, and a more detailed comparison of structural data between calculation and experiment for the crystallographically characterized  $[\text{Mo}_3\text{I}_{12}]^{3-}$  species is presented in Table 5. For comparison, geometry optimizations were also performed using  $C_s$  symmetry, but only minor distortions from the full  $D_{3d}$  symmetry are predicted.

The potential energy curves for each state were generated by systematically varying the metal–metal distance while allowing all remaining structural parameters to be fully optimized. For all species considered, the total bonding energy of the optimized structures is lowest for the BS state, with the  $S = 7/2$  state lying slightly to higher energy and the  $S = 9/2$  state significantly more destabilized. In all cases, the  $S = 9/2$  state has the longest metal–metal distance, but while the BS state exhibits the shortest metal–metal separation for  $[\text{Mo}_3\text{F}_{12}]^{3-}$  and  $[\text{W}_3\text{Cl}_{12}]^{3-}$ , this occurs in the  $S = 7/2$  state for  $[\text{Mo}_3\text{Cl}_{12}]^{3-}$ ,  $[\text{Mo}_3\text{Br}_{12}]^{3-}$ , and  $[\text{Mo}_3\text{I}_{12}]^{3-}$ . The longer Mo–Mo distances for the BS relative to  $S = 7/2$  state for the latter three complexes indicate that the metal–metal interaction in the BS state is weaker than in the  $S = 7/2$  state. Consequently, the electrons involved in metal–metal  $\sigma$  bonding are not fully decoupled, and this has implications in understanding the magnetic behavior of these systems, which is discussed in section 3.4. The same trend in

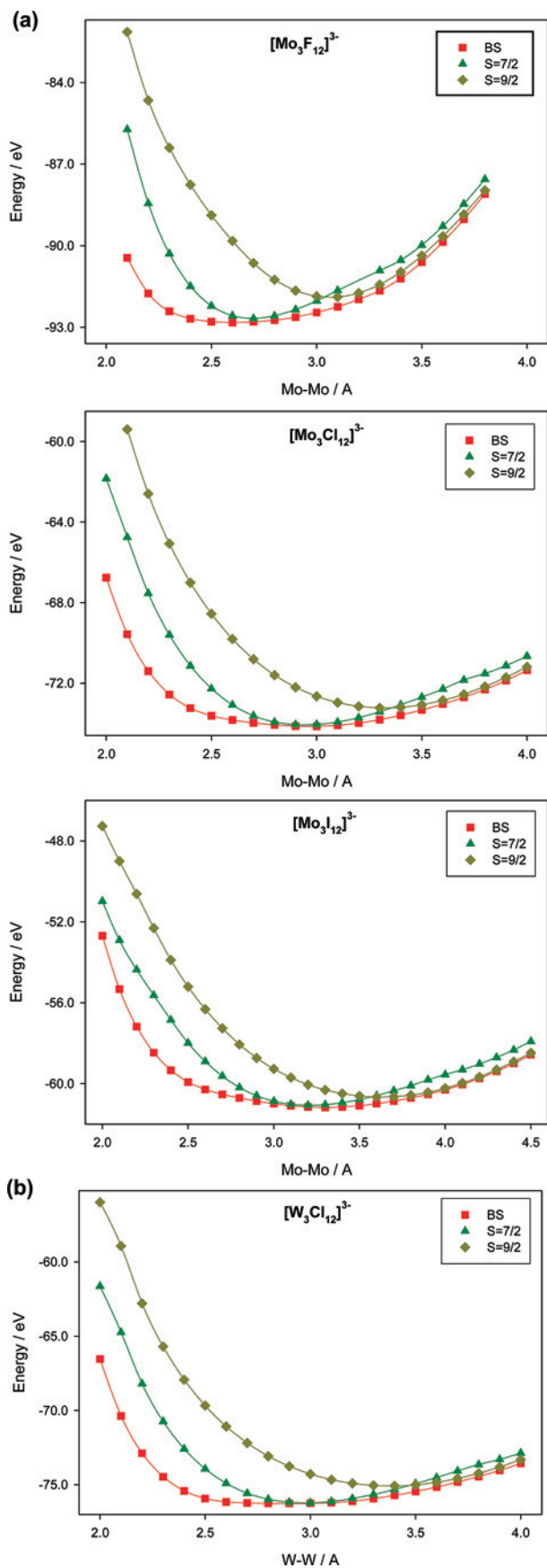


**Figure 3.** Potential energy curves for the BS,  $S = 7/2$ , and  $S = 9/2$  states of the symmetric forms of  $[M_3X_{12}]^{3-}$  species.

**Table 4.** Optimized Metal–Metal Distance (Å) for the BS,  $S = 7/2$ , and  $S = 9/2$  States of  $[Mo_3X_{12}]^{3-}$  ( $X = F, Cl, Br, I$ ) and  $[W_3Cl_{12}]^{3-}$  Systems in (Full)  $D_{3d}$  Symmetry

molecule	BS	$S = 7/2$	$S = 9/2$
$[Mo_3F_{12}]^{3-}$	2.648	2.690	3.063
$[Mo_3Cl_{12}]^{3-}$	2.950	2.938	3.338
$[Mo_3Br_{12}]^{3-}$	3.120	3.049	3.450
$[Mo_3I_{12}]^{3-}$	3.337	3.214	3.643
$[W_3Cl_{12}]^{3-}$	2.938	2.983	3.384

**Table 5.** Comparison of Calculated ( $D_{3d}$  Symmetry) and Observed Structural Parameters for  $[Mo_3I_{12}]^{3-}$

parameter	calculation	experiment
Mo–Mo	3.337 Å	3.258 Å
Mo–I (bridging)	2.781–2.819 Å	2.761–2.825 Å
Mo–I (terminal)	2.776 Å	2.749–2.757 Å
I–Mo–I (bridging)	87–89°	88–91°
I–Mo–I (terminal)	91°	90–91°

metal–metal distances observed in Table 4 for  $[Mo_3X_{12}]^{3-}$  species, progressively increasing from  $X = F$  to  $X = I$ , is also found for the related  $[Mo_2X_9]^{3-}$  dimer series.<sup>16,19</sup>

In earlier publications,<sup>12–26</sup> we have shown that a satisfactory description of the entire range of metal–metal interactions in face-shared  $[M_2X_9]^{z-}$  and edge-shared  $[M_2X_{10}]^{z-}$  dimers can be achieved by means of an approach based on analyzing broken-symmetry potential energy curves in terms of the curves for the corresponding associated states, which arise when one or more subsets of ( $\sigma$ ,  $\pi$ ,  $\delta$ ) metal-based electrons are engaged in metal–metal bonding. In the associated states, the weakly coupled electrons on adjacent metal centers are aligned parallel. The same approach can be extended to the analysis of face-shared  $[M_3X_{12}]^{3-}$  trimers involving the broken-symmetry (BS) state and the  $S = 7/2$  and  $S = 9/2$  associated states.

For all systems, the BS curve lies lowest in energy over the entire range of metal–metal distances investigated, with the curves for the  $S = 7/2$  and  $S = 9/2$  associated states being close or almost coincident with that for the BS state at intermediate and long metal–metal separations, respectively. These results can be rationalized on the basis that the BS state behaves as the antiferromagnetic counterpart of the  $S = 7/2$  state at intermediate metal–metal distances where two electrons are paired in a  $\sigma$  bond across all three metal centers, and the  $S = 9/2$  state at long metal–metal separations where all three metal centers are weakly coupled.

**3.3. Unsymmetric Structures.** Potential energy curves for the unsymmetric forms (Scheme 1) of the  $[M_3X_{12}]^{3-}$  species in the  $M_S = 3/2$  broken-symmetry state were calculated by reducing the molecular symmetry from  $D_{3d}$  to  $C_{3v}$  and systematically varying one of the metal–metal distances while allowing all remaining structural parameters, including the second metal–metal distance, to be fully optimized. The results are shown in Figure 4, where the curves for the symmetric ( $D_{3d}$ ) forms in the broken-symmetry state are also included for comparison.

The curves for the unsymmetric ( $C_{3v}$ ) forms exhibit two minima corresponding to the two possible configurations with alternating short and long metal–metal distances, separated by a barrier that coincides with the minimum in the curves for the symmetric ( $D_{3d}$ ) forms. A comparison of the metal–metal

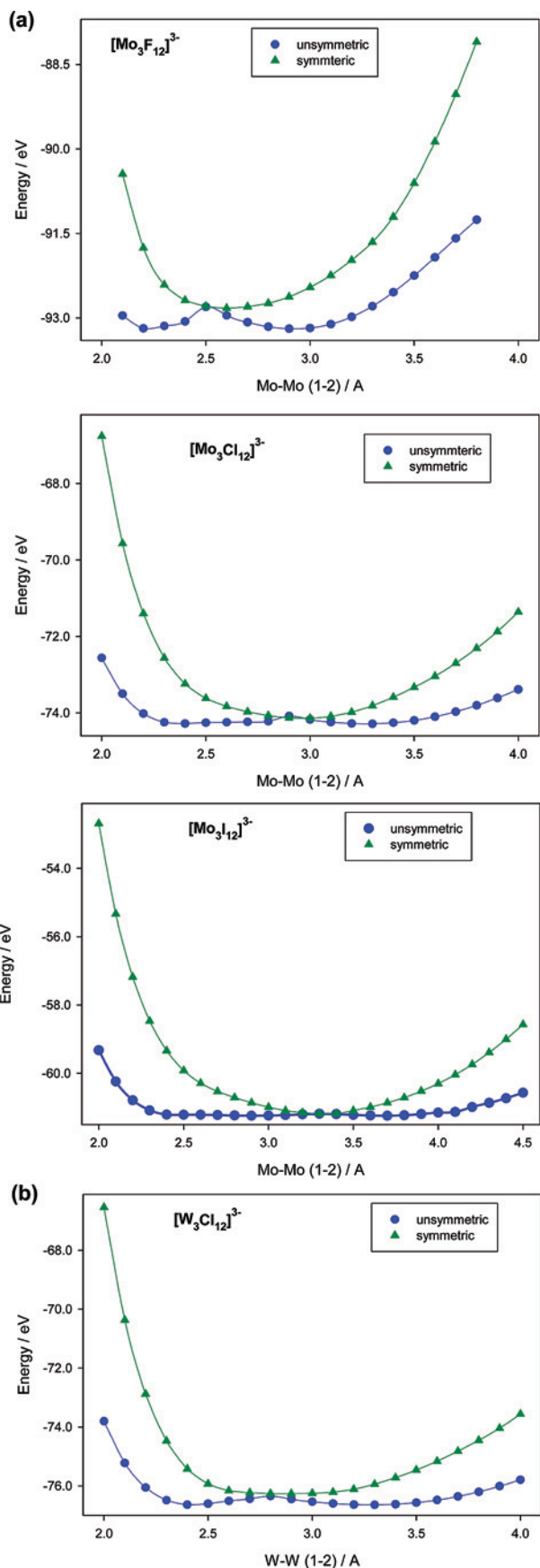


**Figure 4.** Comparison of the broken-symmetry potential energy curves for the symmetric and unsymmetric forms of  $[M_3X_{12}]^{3-}$  species.

**Table 6.** Comparison of Optimized Metal–Metal Distances (M–M in angstroms) and Total Bonding Energy ( $E_B$  in electronvolts) for the Broken-Symmetry ( $M_S = ^3/2$ ) state of the Symmetric ( $D_{3d}$ ) and Unsymmetric ( $C_{3v}$ ) Forms of  $[Mo_3X_{12}]^{3-}$  ( $X = F, Cl, Br, I$ ) and  $[W_3Cl_{12}]^{3-}$  Systems

molecule	symmetry	M–M	$E_B$
$[Mo_3F_{12}]^{3-}$	$D_{3d}$	2.648	–92.89
	$C_{3v}$	2.223, 2.902	–93.19
$[Mo_3Cl_{12}]^{3-}$	$D_{3d}$	2.950	–74.18
	$C_{3v}$	2.367, 3.300	–74.28
$[Mo_3Br_{12}]^{3-}$	$D_{3d}$	3.120	–68.19
	$C_{3v}$	2.402, 3.447	–68.29
$[Mo_3I_{12}]^{3-}$	$D_{3d}$	3.337	–61.18
	$C_{3v}$	2.900, 3.689	–61.24
$[W_3Cl_{12}]^{3-}$	$D_{3d}$	2.938	–76.30
	$C_{3v}$	2.424, 3.291	–76.64

separations and total bonding energy at the respective minima of the  $D_{3d}$  and  $C_{3v}$  curves is given in Table 6.

The short metal–metal distance in the minima of the unsymmetric forms, which ranges from 2.2–2.4 Å, is significantly smaller than the metal–metal distance at the single minima in the symmetric forms, which varies from 2.6 to 3.3 Å. Consequently, the metal–metal interaction in the unsymmetric form is expected to be considerably stronger. It should be noted that although the minimum in the  $C_{3v}$  form of  $[Mo_3I_{12}]^{3-}$  strictly occurs at the relatively long Mo–Mo separation of 2.90 Å, the corresponding curve is essentially flat between approximately 3.10 and 2.40 Å and a second minimum is observed at a Mo–Mo separation of 2.45 Å, which is closer to the values obtained for  $[Mo_3F_{12}]^{3-}$ ,  $[Mo_3Cl_{12}]^{3-}$ , and  $[Mo_3Br_{12}]^{3-}$ .

Plots of the metal–metal based orbitals for the unsymmetric form of  $[Mo_3I_{12}]^{3-}$  (at the short minimum of 2.45 Å) are shown in Figure 5. The qualitative description of these orbitals corresponds to a formal triple bond between the two Mo atoms with the shortest metal–metal separation, while the three remaining electrons are decoupled and localized on the third Mo atom.

The energetic difference between the two structural forms depends on the nature of the ligand and metal. Within the Mo series, the unsymmetric form becomes increasingly stabilized as the ligand identity changes from I through to F. This result is consistent with the shortening of the Mo–Mo bond length and decreasing covalency of the metal–ligand interaction associated with the strengthening of the metal–metal bonding interaction.<sup>19</sup> A comparison of the  $[M_3Cl_{12}]^{3-}$  systems reveals that the relative stability of the unsymmetric ( $C_{3v}$ ) with respect to the symmetric ( $D_{3d}$ ) form, is considerably larger in  $[W_3Cl_{12}]^{3-}$  than  $[Mo_3Cl_{12}]^{3-}$ . An explanation for this difference lies in the fact that, although the metal–metal distances are similar, the more extensive overlap between the W 5d orbitals should lead to a stronger metal–metal interaction and greater relative stabilization.

The unsymmetric ( $C_{3v}$ ) and symmetric ( $D_{3d}$ ) forms of the  $[M_3X_{12}]^{3-}$  systems could, in principle, be considered as an example of bond-stretch isomerism according to the definition proposed by Parkin,<sup>55</sup> which refers to “molecules that

(54) Stranger, R.; Smith, P. W.; Grey, I. E. *Inorg. Chem.* **1989**, *28*, 1271.

(55) Parkin, G. *Chem. Rev.* **1993**, *93*, 887.

(56) Dunbar, K. R.; Pence, L. E. *Acta Crystallogr. C* **1991**, *47*, 23.

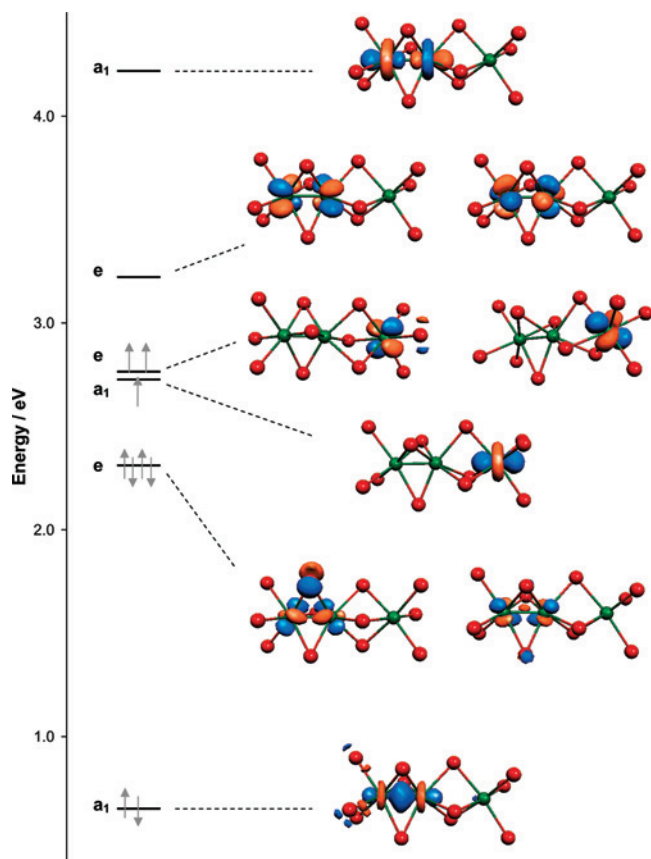


**Figure 5.** Molecular orbital plots for the unsymmetric form of the  $[Mo_3I_{12}]^{3-}$  species.

differ only in the length of one or more bonds". However, as pointed out by Rohmer and Bénard,<sup>1</sup> a complete characterization of isomers requires that the corresponding structures be identified as separate minima.

Vibrational frequency analyses performed for all  $C_{3v}$  and  $D_{3d}$  forms indicate that only the unsymmetric structures are true minima. Calculations on the symmetric forms have been carried out using both numerical and analytical procedures (and for  $[Mo_3I_{12}]^{3-}$  convergence criteria of varying accuracy have also been tested), and imaginary values have been obtained in all cases. The overall results suggest that the symmetric forms can be described as a transition state between the two possible configurations of the unsymmetric forms where the short metal–metal bond alternates from one side of the molecule to the other.

A possible explanation for the fact that the experimentally characterized  $[Mo_3I_{12}]^{3-}$  structure is largely symmetric may lie in the fact that the energetic barrier (Figure 4) for interconversion between the two configurations associated with the unsymmetric form is only approximately  $6 \text{ kJ mol}^{-1}$ . This value actually represents an upper limit to the interconversion as the true  $S = 3/2$  ground-state for the symmetric structure will lie lower in energy than the BS state. Since the interconversion should be a relatively facile process at room temperature, the experimentally observed structure may correspond to the symmetric average of the two unsymmetric configurations. Isolation of an unsymmetric  $[M_3X_{12}]^{3-}$  species may be feasible at low temperatures, or for systems such as

$[Mo_3F_{12}]^{3-}$  and  $[W_3Cl_{12}]^{3-}$ , which exhibit significantly larger barriers to interconversion.

It should be noted that although the minima for the unsymmetric forms correspond to pure  $S = 3/2$  spin states, as the unpaired electrons only reside on a single (decoupled) metal center, the broken-symmetry minima associated with the symmetric forms are not pure spin states. In order to fully appreciate this aspect and its possible effect on the relative stabilities of the symmetric and unsymmetric forms of  $[M_3X_{12}]^{3-}$  species, it is necessary to examine the magnetic coupling in these systems in more detail.

**3.4. Magnetic Properties.** Magnetic susceptibility data have been measured for the  $[Mo_3X_{12}]^{3-}$  ( $X = Cl, Br, I$ ) systems.<sup>8,9</sup> The reported solid state magnetic moments for  $[(n-C_4H_9)_4N]_3[Mo_3Cl_{12}]$  range from  $1.34 \mu_B$  at 103 K to  $2.02 \mu_B$  at 302 K.<sup>9</sup> Interestingly, the solution-based measurements for the same compound are somewhat higher, 2.1 and  $2.5 \mu_B$  at 189 and 291 K, respectively. The discrepancy between the solid state and solution measurements was attributed to intermolecular antiferromagnetic coupling effects in the former resulting in reduced magnetic moments, particularly at low temperatures. Fettinger and co-workers<sup>8</sup> have reported the room temperature magnetic moments for  $[PPh_4]_3[Mo_3I_{12}]$ ,  $[NPr_4]_3[Mo_3I_{12}]$ , and  $[PPh_4]_3[Mo_3Br_{12}]$  as 3.17, 3.36, and  $2.60 \mu_B$ , respectively. The magnetic moments for the iodide complexes are close to that expected for three unpaired electrons, in agreement with the  $S = 3/2$  ground-state predicted from the calculations discussed in previous sections. Clearly, the room temperature magnetic moments of approximately 2.0 ( $X = Cl$ ), 2.6 ( $X = Br$ ), and  $3.3 \mu_B$  ( $X = I$ ) for  $[Mo_3X_{12}]^{3-}$ , display a strong dependence on the halide ligand, with the antiferromagnetic coupling between the metal centers becoming progressively weaker as the halide group is descended.

Fettinger and co-workers<sup>8</sup> have modeled the temperature dependence of the magnetic moment for  $[PPh_4]_3[Mo_3I_{12}]$  and  $[PPh_4]_3[Mo_3Br_{12}]$  between 1.7 and 300 K using a Heisenberg spin Hamiltonian for the trinuclear system of the form,

$$H = -2J_{12}[(S_1S_2) + (S_2S_3)] - 2J_{13}(S_1S_3) \quad (2)$$

with  $S_1 = S_3 = 1$  and  $S_2 = 3/2$ . In this expression,  $J_{12}$  measures the coupling between the central Mo atom and both terminal Mo atoms, while  $J_{13}$  represents the coupling between the two terminal Mo centers. Using this model, the best fit to the susceptibility data was obtained for  $J_{12} = -521 \text{ cm}^{-1}$  and  $J_{13} = 5.1 \text{ cm}^{-1}$  for  $[PPh_4]_3[Mo_3I_{12}]$ .

The model used by Fettinger and co-workers assumes that two of the nine metal-based electrons are not involved in the antiferromagnetic coupling due to their participation in a two-electron three-center  $\sigma$  bond between the metal atoms. Thus, the antiferromagnetic behavior was attributed to the remaining seven electrons, which occupy essentially non-bonding orbitals. The validity of this coupling mode can be assessed by an examination of the unpaired electron density from a Mulliken population analysis, the results of which are given in Table 7 for  $[Mo_3X_{12}]^{3-}$  ( $X = I, Br, Cl, F$ ) and  $[W_3Cl_{12}]^{3-}$ . For  $[Mo_3I_{12}]^{3-}$ , the metal spin densities of 2.68

**Table 7.** Metal Spin Densities ( $\rho$ ) from a Mulliken Population Analysis for the BS,  $S = 7/2$ , and  $S = 9/2$  States in  $[\text{Mo}_3\text{X}_{12}]^{3-}$  ( $\text{X} = \text{I}, \text{Br}, \text{Cl}, \text{F}$ ) and  $[\text{W}_3\text{Cl}_{12}]^{3-}$  Systems in (Full)  $D_{3d}$  Symmetry

molecule	spin state	$\rho(M_1) = \rho(M_3)$	$\rho(M_2)$
$[\text{Mo}_3\text{I}_{12}]^{3-}$	BS	2.40	-2.16
	$S = 7/2$	2.24	1.66
	$S = 9/2$	2.68	2.70
$[\text{Mo}_3\text{Br}_{12}]^{3-}$	BS	2.38	-2.15
	$S = 7/2$	2.25	1.71
	$S = 9/2$	2.68	2.73
$[\text{Mo}_3\text{Cl}_{12}]^{3-}$	BS	2.32	-2.06
	$S = 7/2$	2.23	1.73
	$S = 9/2$	2.68	2.72
$[\text{Mo}_3\text{F}_{12}]^{3-}$	BS	2.39	-2.10
	$S = 7/2$	2.33	1.84
	$S = 9/2$	2.82	2.88
$[\text{W}_3\text{Cl}_{12}]^{3-}$	BS	2.23	-1.96
	$S = 7/2$	2.19	1.72
	$S = 9/2$	2.64	2.70

(terminal Mo) and 2.70 (central Mo) for the  $S = 9/2$  state are consistent with approximately three unpaired electrons on each metal, once due consideration is given to metal–ligand covalency effects. The total unpaired spin density of 6.14 for the  $S = 7/2$  state compared to 8.06 for  $S = 9/2$ , is consistent with the pairing of approximately two electrons in the metal–metal  $\sigma$  bond, but the individual spin densities of 2.24 (terminal Mo) and 1.66 (central Mo) indicate that electron density is lost on all three metal centers, approximately 0.5 electrons from each terminal Mo atom and 1.0 electron from the central Mo atom. Thus, the spin densities are not compatible with the assignment of  $S_1 = S_3 = 1$  and  $S_2 = 3/2$  used by Fettinger and co-workers, where each terminal center loses one electron while the central Mo atom remains unchanged. A similar argument also applies to the other complexes examined in this study in that electron density is lost from all three metals in progressing from the  $S = 9/2$  to  $S = 7/2$  states.

In the broken-symmetry state for the symmetric structure, which most accurately reflects the magnetic coupling between the metal centers in the true antiferromagnetic ground state, the spin density on all three metal centers in  $[\text{Mo}_3\text{I}_{12}]^{3-}$  increases relative to the  $S = 7/2$  state, and the total unpaired spin density of 6.96 is over 0.8 electrons larger than that for the  $S = 7/2$  state. The increase in the unpaired spin density for the BS state is consistent with the 0.12 Å increase in the Mo–Mo distance compared to the  $S = 7/2$  state and indicates that the metal–metal interaction in  $[\text{Mo}_3\text{I}_{12}]^{3-}$  is somewhat weaker than that predicted for a formal bond order of 0.5 between the Mo atoms. The spin densities in the BS state imply that the electrons occupying the  $a_{1g}$  metal–metal  $\sigma$  bonding orbital are not fully paired and therefore participate in antiferromagnetic coupling in the metal cluster. Consequently, a model that considers all nine electrons involved in magnetic interactions is likely to be closer to the real coupling mode than the  $\sigma$ -bonded model with  $S_1 = S_3 = 1$  and  $S_2 = 3/2$ . Accordingly, in the analysis to follow, we make use of the broken-symmetry approach combined with spin projection to determine the relative energies of the low-lying spin states in  $[\text{Mo}_3\text{I}_{12}]^{3-}$  and the related  $[\text{Mo}_3\text{X}_{12}]^{3-}$  ( $\text{X} = \text{Br}, \text{Cl}, \text{F}$ ) and  $[\text{W}_3\text{Cl}_{12}]^{3-}$  complexes.

In the broken-symmetry approach, one or more antiferromagnetic states are formed by locating the spin-up and spin-down electrons on different metal centers. Spin projection allows the energy differences involving the broken-symmetry and high-spin states to be expressed in terms of the various exchange coupling ( $J_{ij}$ ) parameters. Once the  $J_{ij}$  values have been determined, they can be used to calculate the energy of the pure spin states, including the ground state, on the basis of a Heisenberg spin Hamiltonian formalism. For trinuclear species, and polynuclear complexes in general, the procedure is complicated by the fact that more than one broken-symmetry state is possible due to different ways of coupling the spins on the metal centers. In the case of  $[\text{M}_3\text{X}_{12}]^{3-}$  systems, two broken-symmetry states with  $M_S = 3/2$  are possible. A symmetric broken-symmetry ( $\text{BS}_{\text{sym}}$ ) state results when the electrons on the central metal atom are aligned antiparallel to those on the terminal metal centers (and corresponds to the broken-symmetry state for the symmetric ( $D_{3d}$ ) structure discussed in the previous sections), while an asymmetric broken-symmetry ( $\text{BS}_{\text{asym}}$ ) state is formed when the electrons on the central atom are aligned parallel to one terminal center but antiparallel to the other center. In general, the broken-symmetry state of lowest energy most closely resembles the spin coupling arrangement existing in the ground state.

For polynuclear spin coupled complexes, the energy of the broken-symmetry states is given by

$$H = \sum_{ij} -2J_{ij} \langle \hat{S}_i \cdot \hat{S}_j \rangle \quad (3)$$

where the expectation values  $\langle \hat{S}_i \cdot \hat{S}_j \rangle$  correspond to  $+S_i S_j$  and  $-S_i S_j$  for parallel and antiparallel alignment of spins on metal centers  $M_i$  and  $M_j$ , respectively. For a symmetric linear trinuclear cluster with  $S_1 = S_2 = S_3 = 3/2$ , application of the above equation leads to the following expressions for the energy differences between the high-spin  $S = 9/2$  and symmetric ( $\text{BS}_{\text{sym}}$ ) and asymmetric ( $\text{BS}_{\text{asym}}$ ) broken-symmetry states,

$$E(9/2) - E(\text{BS}_{\text{sym}}) = -18J_{12} \quad (4)$$

$$E(9/2) - E(\text{BS}_{\text{asym}}) = -9J_{12} - 9J_{13} \quad (5)$$

It should be noted that although the  $\text{BS}_{\text{asym}}$  state has an asymmetric distribution of the spin-up and spin-down electron density on the metal centers, its energy is calculated using the symmetric  $D_{3d}$  geometry of the  $[\text{M}_3\text{X}_{12}]^{3-}$  complex. From the above expressions, the values of  $J_{12}$  and  $J_{13}$  can be determined and substituted into the following equation based on the solution of the Heisenberg spin Hamiltonian given in equation 2,

$$E(S', S) = -J_{12}[S(S+1)] + J_{12}[S'(S'+1)] - J_{13}[S'(S'+1)] \quad (6)$$

in order to calculate the energies of the total spin ( $S$ ) states for the trinuclear system. In this equation,  $S' = S_1 + S_3$  and  $S = S' + S_2$ , and therefore,  $S'$  can take the values of 0, 1, 2, and 3 while the total spin has values of  $S = 1/2, 3/2, 5/2, 7/2$ , and  $9/2$ . From eqs 4 and 6, we can show that

**Table 8.** Spin State Energies (eV) and Magnetic Exchange Parameters ( $J_{12}$  and  $J_{13}$  ( $\text{cm}^{-1}$ )) for  $[\text{Mo}_3\text{X}_{12}]^{3-}$  ( $X = \text{I, Br, Cl, F}$ ) and  $[\text{W}_3\text{Cl}_{12}]^{3-}$  Systems

molecule	spin state <sup>a</sup>	energy	$J_{12}$ <sup>b</sup>	$J_{13}$ <sup>b</sup>
$[\text{Mo}_3\text{I}_{12}]^{3-}$	$S = 9/2$	-60.7235	-207	+17
	$\text{BS}_{\text{sym}} (D_{3d})$	-61.1846		
	$\text{BS}_{\text{asym}}$	-60.9350		
	$S = 3/2$	-61.2614		
$[\text{Mo}_3\text{Br}_{12}]^{3-}$	$\text{BS}_{\text{sym}} (C_{3v})$	-61.2396	-303	-48
	$S = 9/2$	-67.5166		
	$\text{BS}_{\text{sym}} (D_{3d})$	-68.1921		
	$\text{BS}_{\text{asym}}$	-67.9080		
$[\text{Mo}_3\text{Cl}_{12}]^{3-}$	$S = 3/2$	-68.3047	-388	-128
	$\text{BS}_{\text{sym}} (C_{3v})$	-68.2935		
	$S = 9/2$	-73.3163		
	$\text{BS}_{\text{sym}} (D_{3d})$	-74.1827		
$[\text{Mo}_3\text{F}_{12}]^{3-}$	$\text{BS}_{\text{asym}}$	-73.8918	-377	-22
	$S = 3/2$	-74.3270		
	$\text{BS}_{\text{sym}} (C_{3v})$	-74.2842		
	$S = 9/2$	-92.0524		
$[\text{W}_3\text{Cl}_{12}]^{3-}$	$\text{BS}_{\text{sym}} (D_{3d})$	-92.8939	-507	-268
	$\text{BS}_{\text{asym}}$	-92.4973		
	$S = 3/2$	-93.0342		
	$\text{BS}_{\text{sym}} (C_{3v})$	-93.1936		
$[\text{W}_3\text{Cl}_{12}]^{3-}$	$S = 9/2$	-75.1690	-507	-268
	$\text{BS}_{\text{sym}} (D_{3d})$	-76.3011		
	$\text{BS}_{\text{asym}}$	-76.0346		
	$S = 3/2$	-76.4898		
$[\text{W}_3\text{Cl}_{12}]^{3-}$	$\text{BS}_{\text{sym}} (C_{3v})$	-76.6423		

<sup>a</sup> Energy of  $S = 3/2$  state obtained by spin projection using eq 7. <sup>b</sup>  $J_{12}$  and  $J_{13}$  values calculated using eqs 4 and 5.

the following relationships holds between the broken-symmetry ( $\text{BS}_{\text{sym}}$ ) state and the lowest lying  $S = 3/2$  and  $S = 1/2$  states,

$$E(\text{BS}_{\text{sym}}) - E(3/2) = -3J_{12} \quad (7)$$

$$E(\text{BS}_{\text{sym}}) - E(1/2) = -6J_{13} \quad (8)$$

On the basis of eqs 7 and 8, for symmetric structures, the  $S = 3/2$  is the ground-state as long as  $-J_{12} > -2J_{13}$ . The energies of the high-spin  $S = 9/2$  state, the  $\text{BS}_{\text{sym}}$  and  $\text{BS}_{\text{asym}}$  broken-symmetry states in  $D_{3d}$  symmetry, and the  $\text{BS}_{\text{sym}}$  broken-symmetry state in  $C_{3v}$  symmetry are given in Table 8 for the  $[\text{M}_3\text{X}_{12}]^{3-}$  complexes examined in this study. Also included are the values of  $J_{12}$  and  $J_{13}$  calculated using eqs 4 and 5, and the spin-projected energy of the  $S = 3/2$  ground state for the symmetric ( $D_{3d}$ ) structure obtained from eq 7.

For  $[\text{Mo}_3\text{I}_{12}]^{3-}$ , the calculated values of  $J_{12} = -207 \text{ cm}^{-1}$  and  $J_{13} = 17 \text{ cm}^{-1}$  indicate moderately large antiferromagnetic coupling between adjacent metal centers but weak ferromagnetic interactions between the two terminal metal atoms. The calculated value of  $J_{12}$  is less than half-the reported value of  $-521 \text{ cm}^{-1}$ , but the latter is based on fitting the magnetic data to a Heisenberg model with  $S_1 = S_3 = 1$  and  $S_2 = 3/2$ , which, as mentioned above, is not consistent with the unpaired spin densities given in Table 5. The  $-J_{12}$  values for  $[\text{Mo}_3\text{F}_{12}]^{3-}$  and  $[\text{Mo}_3\text{Cl}_{12}]^{3-}$  are similar and close to  $380 \text{ cm}^{-1}$ , while  $-J_{12}$  for  $[\text{W}_3\text{Cl}_{12}]^{3-}$  is approximately  $120 \text{ cm}^{-1}$  greater. The more antiferromagnetic  $J_{12}$  values for  $[\text{Mo}_3\text{Br}_{12}]^{3-}$ ,  $[\text{Mo}_3\text{Cl}_{12}]^{3-}$ ,  $[\text{Mo}_3\text{F}_{12}]^{3-}$ , and  $[\text{W}_3\text{Cl}_{12}]^{3-}$  relative to  $[\text{Mo}_3\text{I}_{12}]^{3-}$  are in accord with the reduced metal-metal separations calculated for these complexes. With the exception of the fluoride complex, a similar trend is also observed for  $J_{13}$ . However, the much larger antiferromagnetic values of  $J_{13}$  for  $[\text{Mo}_3\text{Cl}_{12}]^{3-}$  and, in particular,  $[\text{W}_3\text{Cl}_{12}]^{3-}$ , may

indicate that the assumption of all nine metal-based electrons being weakly coupled is less valid. If this is the case, then the calculated values of  $J_{12}$  will be overestimated and this will need to be taken into consideration in the analysis to follow. Some indication of this overestimation can be obtained by comparing our calculated value of  $J_{12} = -388 \text{ cm}^{-1}$  for  $[\text{Mo}_3\text{Cl}_{12}]^{3-}$  with the value of  $J_{12} = -245 \text{ cm}^{-1}$  obtained by Delphin and co-workers<sup>9</sup> on fitting the temperature dependence of the magnetic moments for  $[(n\text{-C}_4\text{H}_9)_4\text{N}]_3[\text{Mo}_3\text{Cl}_{12}]$  to a two-state ( $S = 1/2, 3/2$ ) magnetic model. The data in Table 7 show that the total unpaired spin density drops by 1.18, 1.38, 1.56, and 1.64 electrons from the  $S = 9/2$  state to the  $\text{BS}_{\text{sym}}$  state for  $[\text{Mo}_3\text{Br}_{12}]^{3-}$ ,  $[\text{Mo}_3\text{Cl}_{12}]^{3-}$ ,  $[\text{W}_3\text{Cl}_{12}]^{3-}$ , and  $[\text{Mo}_3\text{F}_{12}]^{3-}$ , respectively, suggesting that the metal-metal interaction in these systems is stronger than in  $[\text{Mo}_3\text{I}_{12}]^{3-}$ , for which the equivalent result is only 1.10 electrons. The reduction in the room-temperature magnetic moments reported for both  $[\text{Mo}_3\text{Br}_{12}]^{3-}$  and  $[\text{Mo}_3\text{Cl}_{12}]^{3-}$  compared to  $[\text{Mo}_3\text{I}_{12}]^{3-}$  is consistent with this conclusion.

From the energy values given in Table 8, the spin projected  $S = 3/2$  state for the symmetric structure lies lowest in energy for both  $[\text{Mo}_3\text{I}_{12}]^{3-}$  and  $[\text{Mo}_3\text{Br}_{12}]^{3-}$ . However, the fact that the broken-symmetry  $\text{BS}_{\text{sym}}$  state for the unsymmetric structures lies at most 0.02 eV to higher energy suggests that the potential surface for the  $S = 3/2$  state is relatively flat in both complexes. Consequently, interconversion between the two energetically equivalent unsymmetric configurations should result in an averaged structure that is symmetric at room temperature, in agreement with the approximately  $D_{3d}$  geometry observed experimentally for  $[\text{Mo}_3\text{I}_{12}]^{3-}$ . This description is consistent with the reported crystal structure for this complex,<sup>8</sup> where the shape of the thermal ellipsoid for the central Mo atom is significantly distorted toward the Mo atoms on either side. A similar outcome is also predicted for  $[\text{Mo}_3\text{Cl}_{12}]^{3-}$  with the spin projected  $S = 3/2$  state lying 0.04 eV lower than the  $\text{BS}_{\text{sym}}$  state for the unsymmetric structure but, as noted above, this ignores the possibility that  $J_{12}$  may be overestimated on the basis of the moderately large antiferromagnetic  $J_{13}$  value calculated for this complex. However, even if this is the case, a value of  $-J_{12} > 273 \text{ cm}^{-1}$  will result in the  $S = 3/2$  state being the ground-state and, given that the Mo-Mo distance for the  $[\text{Mo}_3\text{Cl}_{12}]^{3-}$  is nearly 0.4 Å shorter than for  $[\text{Mo}_3\text{I}_{12}]^{3-}$ , a value of at least this magnitude is not unreasonable. A different scenario arises for  $[\text{Mo}_3\text{F}_{12}]^{3-}$  and  $[\text{W}_3\text{Cl}_{12}]^{3-}$ . For these complexes, the  $\text{BS}_{\text{sym}}$  state for the unsymmetric structure lies lowest in energy, approximately 0.15 eV below the spin projected  $S = 3/2$  state, and consequently, both complexes are predicted to possess unsymmetric structures with one short and one long metal-metal distance. Any overestimation of  $J_{12}$  for these complexes will only serve to further stabilize the  $\text{BS}_{\text{sym}}$  state for the unsymmetric structure relative to the  $S = 3/2$  state. Given that the energy gap between the unsymmetric and symmetric forms is not insignificant, at least  $1200 \text{ cm}^{-1}$ , it

seems likely that even the room temperature structures of these complexes should remain unsymmetric.

Finally, it is worthwhile noting that although both the symmetric and unsymmetric structures are predicted to possess  $S = 3/2$  ground states, a low-lying  $S = 1/2$  state is possible in the unsymmetric case if the  $S = 3/2$  state of the more isolated Mo center is antiferromagnetically coupled to either the  $S = 1$  or  $S = 2$  states associated with the two remaining metal–metal bonded Mo centers. Both the  $S = 1$  and  $S = 2$  states involve unpairing electrons from the metal–metal ( $\delta/\pi$ ) bonding orbitals into the corresponding antibonding orbitals. A similar coupling scenario was proposed recently in order to explain the unusual temperature dependence of the structure and magnetic properties of the linear tricobalt  $[\text{Co}_3(\mu_3\text{-dpa})_4\text{Cl}_2]$  system.<sup>2</sup> To determine the feasibility of this type of coupling arrangement, we have calculated the energy of the broken-symmetry ( $M_S = 1/2$ ) state for the  $[(S = 3/2) \times (S = 2)]$  system in both  $[\text{Mo}_3\text{I}_{12}]^{3-}$  and  $[\text{Mo}_3\text{Cl}_{12}]^{3-}$ . The corresponding  $[(S = 3/2) \times (S = 1)]$  system is not a single determinant in trigonal ( $C_{3v}$ ) symmetry and therefore is not amenable to calculation by density functional methods. The geometry optimized  $[(S = 3/2) \times (S = 2)]$  broken-symmetry state is calculated to lie 0.13 and 0.21 eV above the unsymmetric  $S = 3/2$  ground-state in  $[\text{Mo}_3\text{I}_{12}]^{3-}$  and  $[\text{Mo}_3\text{Cl}_{12}]^{3-}$ , respectively. Not unexpectedly, the short Mo–Mo distance in these complexes increases to 2.972 and 2.794 Å for the iodide and chloride complexes, respectively, relative to the unsymmetric  $S = 3/2$  structures, due to electrons occupying ( $\delta/\pi$ ) antibonding orbitals. Although these energy gaps are not large, they are nonetheless not small enough to result in significant population of the associated  $S = 1/2$  state, particularly for the chloride complex, which is therefore unlikely to be contributing to the magnetic properties of these complexes at low temperatures. Consequently, the reduced magnetic moments observed in these systems must be attributed to intermolecular antiferromagnetic coupling effects, as originally suggested by Delphin and co-workers.<sup>9</sup>

**3.5. Methodological Comparisons.** The results obtained from [LDA/TZP] and [PBE/ZC/TZ2P] calculations for the BS,  $S = 7/2$ , and  $S = 9/2$  states of the symmetric form of  $[\text{Mo}_3\text{I}_{12}]^{3-}$  (Table 3) have been compared and discussed in section 3.1. An additional comparison between these two approaches is presented in Table 9, which includes data for metal–metal distances, energetics, and  $J_{12}$  values for all species investigated in this work.

The optimized metal–metal distances obtained by the two computational approaches exhibit, in general, small differences, with the exception of the  $C_{3v}$  results for  $[\text{Mo}_3\text{Cl}_{12}]^{3-}$  and  $[\text{Mo}_3\text{Br}_{12}]^{3-}$ , and the  $D_{3d}$  result for  $[\text{W}_3\text{Cl}_{12}]^{3-}$ . As discussed in previous sections, these discrepancies arise due to the fact that, in some cases, the potential energy curves are rather flat and the total bonding energy values show only minor variations across a relatively large range of metal–metal separations.

The  $J_{12}$  values for the Mo species are largely similar, but a relatively significant difference is found between the two approaches in the case of the W system. However, these results

**Table 9.** Comparison of Calculated Data for Selected Structural Parameters (M–M in angstroms), energetics ( $E$  in electronvolts), and magnetic properties ( $J_{12}$  in centimeters<sup>-1</sup>) of  $[\text{Mo}_3\text{X}_{12}]^{3-}$  ( $X = \text{I}, \text{Br}, \text{Cl}, \text{F}$ ) and  $[\text{W}_3\text{Cl}_{12}]^{3-}$  Systems

molecule	parameter	LDA/TZP	PBE/ZC/TZ2P <sup>a</sup>
$[\text{Mo}_3\text{I}_{12}]^{3-}$	M–M [BS <sub>sym</sub> ( $D_{3d}$ )]	3.34	3.31
	M–M [BS <sub>sym</sub> ( $C_{3v}$ )]	2.90, 3.69	2.91, 3.65
	$E$ [ $S = 3/2$ ]	-61.26	-67.81
	$E$ [BS <sub>sym</sub> ( $C_{3v}$ )]	-61.24	-67.76
	$J_{12}$	-207	-192
$[\text{Mo}_3\text{Br}_{12}]^{3-}$	M–M [BS <sub>sym</sub> ( $D_{3d}$ )]	3.12	3.10
	M–M [BS <sub>sym</sub> ( $C_{3v}$ )]	2.40, 3.45	2.84, 3.26
	$E$ [ $S = 3/2$ ]	-68.30	-75.45
	$E$ [BS <sub>sym</sub> ( $C_{3v}$ )]	-68.29	-75.34
	$J_{12}$	-303	-300
$[\text{Mo}_3\text{Cl}_{12}]^{3-}$	M–M [BS <sub>sym</sub> ( $D_{3d}$ )]	2.95	2.92
	M–M [BS <sub>sym</sub> ( $C_{3v}$ )]	2.37, 3.30	2.72, 3.09
	$E$ [ $S = 3/2$ ]	-74.33	-82.61
	$E$ [BS <sub>sym</sub> ( $C_{3v}$ )]	-74.28	-82.48
	$J_{12}$	-388	-372
$[\text{Mo}_3\text{F}_{12}]^{3-}$	M–M [BS <sub>sym</sub> ( $D_{3d}$ )]	2.65	2.59
	M–M [BS <sub>sym</sub> ( $C_{3v}$ )]	2.22, 2.90	2.17, 2.88
	$E$ [ $S = 3/2$ ]	-93.03	-103.25
	$E$ [BS <sub>sym</sub> ( $C_{3v}$ )]	-93.19	-103.28
	$J_{12}$	-377	-374
$[\text{W}_3\text{Cl}_{12}]^{3-}$	M–M [BS <sub>sym</sub> ( $D_{3d}$ )]	2.94	2.73
	M–M [BS <sub>sym</sub> ( $C_{3v}$ )]	2.42, 3.29	2.40, 3.18
	$E$ [ $S = 3/2$ ]	-76.49	-81.02
	$E$ [BS <sub>sym</sub> ( $C_{3v}$ )]	-76.64	-80.97
	$J_{12}$	-507	-672

<sup>a</sup> The ZC label indicates inclusion of ZORA and COSMO corrections.

are consistent with the trends obtained for the  $[\text{M}_2\text{X}_9]^{2-}$  dimers, which show closer agreement between the [LDA/TZP] and [PBE/ZC/TZ2P] predictions for Mo than W systems.

The trends in relative energy differences between the symmetric ( $S = 3/2$ ) and unsymmetric (BS<sub>sym</sub> ( $C_{3v}$ )) structures are somewhat different for [LDA/TZP] and [PBE/ZC/TZ2P] calculations, with the latter method favoring the symmetric ( $D_{3d}$ ) forms more strongly. This result is particularly significant in the case of  $[\text{Mo}_3\text{F}_{12}]^{3-}$  and  $[\text{W}_3\text{Cl}_{12}]^{3-}$ , which are expected to possess the strongest metal–metal interactions. However, for example, the [PBE/ZC/TZ2P] calculations predict largely the same result for  $[\text{W}_3\text{Cl}_{12}]^{3-}$  and  $[\text{Mo}_3\text{I}_{12}]^{3-}$  (which represent two rather opposite cases), with the symmetric ( $D_{3d}$ ) form slightly favored over the unsymmetric ( $C_{3v}$ ) form. In contrast, the [LDA/TZP] results appear more consistent with qualitative chemical bonding arguments, in that for  $[\text{Mo}_3\text{F}_{12}]^{3-}$  and  $[\text{W}_3\text{Cl}_{12}]^{3-}$ , the unsymmetric ( $C_{3v}$ ) structures are favored, whereas for  $[\text{Mo}_3\text{Cl}_{12}]^{3-}$ ,  $[\text{Mo}_3\text{Br}_{12}]^{3-}$ , and  $[\text{Mo}_3\text{I}_{12}]^{3-}$ , in which the relative strength of metal–metal bonding should have less influence, the two structural forms show more similar relative stability.

#### 4. Conclusion

The electronic structures and metal–metal interactions in trinuclear face-shared  $[\text{M}_3\text{X}_{12}]^{3-}$  species of Mo ( $X = \text{F}, \text{Cl}, \text{Br}, \text{I}$ ) and W ( $X = \text{Cl}$ ) have been investigated using density functional theory. The structures and relative energies of both symmetric and unsymmetric forms possessing  $D_{3d}$  and  $C_{3v}$  molecular symmetry, respectively, have been explored on the basis of calculations involving the antiferromagnetic ( $M_S = 3/2$ ) broken-symmetry state and  $S = 7/2$  and  $S = 9/2$  spin states arising from the

coupling of the individual  $d^3$  metal atoms. The  $S = 3/2$  state, in either the symmetric or unsymmetric forms, is predicted to be the ground-state in all five systems.

Although a bonding analysis of  $[Mo_3I_{12}]^{3-}$  indicates that the metal–metal interaction qualitatively corresponds to a two-electron three-center  $\sigma$  bond between the Mo atoms and, consequently, to a formal Mo–Mo bond order of 0.5, the actual nature of the interaction is likely to be much weaker, due the relatively long metal–metal separation for this species. The calculated spin densities in the broken-symmetry state are consistent with this description and suggest that the electrons in the metal–metal  $\sigma$  bond are not fully paired and therefore participate in antiferromagnetic interactions between the metal centers. The same observation applies to  $[Mo_3F_{12}]^{3-}$ ,  $[Mo_3Cl_{12}]^{3-}$ , and  $[W_3Cl_{12}]^{3-}$ , but both the spin densities and shorter metal–metal distances indicate that the metal–metal interaction is stronger in these systems.

Assuming a weakly coupled model, the  $S = 3/2$  symmetric structure is found to be the ground-state for both  $[Mo_3I_{12}]^{3-}$  and  $[Mo_3Br_{12}]^{3-}$  but the unsymmetric  $S = 3/2$  structure is almost coincident in energy. Thus, the potential energy surface for the  $S = 3/2$  state is expected to be relatively flat in both complexes and consequently, interconversion between the two energetically equivalent unsymmetric configurations should result in an averaged structure that is symmetric at room temperature.

Although the weakly coupled model holds reasonably well for  $[Mo_3I_{12}]^{3-}$  and  $[Mo_3Br_{12}]^{3-}$ , the reduced spin densities,

shorter metal–metal distances, and moderately large  $J_{13}$  values indicate that this assumption is less valid for  $[Mo_3F_{12}]^{3-}$ ,  $[Mo_3Cl_{12}]^{3-}$ , and  $[W_3Cl_{12}]^{3-}$  and, as a consequence, the calculated  $J_{12}$  values for these complexes may be overestimated. In the case of  $[Mo_3F_{12}]^{3-}$  and  $[W_3Cl_{12}]^{3-}$ , even the exaggerated  $J_{12}$  values are not enough to overturn the unsymmetric  $S = 3/2$  state from being the ground-state and, as a result, both complexes are predicted to have unsymmetric structures with strong multiple bonding between two metal centers. The situation for  $[Mo_3Cl_{12}]^{3-}$  is less obvious. A symmetric structure is predicted on the basis of the calculated  $J_{12}$  value, with the unsymmetric structure lying  $345\text{ cm}^{-1}$  to higher energy. Consideration of the fact that  $J_{12}$  is probably overestimated will reduce this gap but not enough to reverse the energetic ordering of these two states. A likely scenario is that, analogous to  $[Mo_3I_{12}]^{3-}$  and  $[Mo_3Br_{12}]^{3-}$ , the unsymmetric structure will be thermally accessible so that, at room temperature, interconversion between the two equivalent unsymmetric forms will result in an averaged structure that is symmetric.

**Acknowledgment.** The authors gratefully acknowledge the Australian Research Council for financial support and the Australian National University for access to the APAC (Australian Partnership for Advanced Computing) super-computing facilities.

IC702070Z